A scalable and modular computational pipeline for axonal connectomics: automated tracing and assembly of axons across serial sections

Russel Torres[1,†], Kevin Takasaki[1,†], Olga Gliko[1,†], Connor Laughland[1], Wan-Qing Yu[1], Emily Turschak[1], Ayana Hellevik[1], Pooja Balaram[1], Eric Perlman[1], Uygar Sümbül[1], and R. Clay Reid[1,*]

[1]Allen Institute for Brain Science, Seattle, WA
[†]Equal contributors
*Correspondence to: clayr@alleninstitute.org

Abstract

Progress in histological methods and in microscope technology has enabled dense staining and imaging of axons over large brain volumes, but tracing axons over such volumes requires new computational tools for 3D reconstruction of data acquired from serial sections. We have developed a computational pipeline for automated tracing and volume assembly of densely stained axons imaged over serial sections, which leverages machine learning-based segmentation to enable stitching and alignment with the axon traces themselves. We validated this segmentation-driven approach to volume assembly and alignment of individual axons over centimeter-scale serial sections and show the application of the output traces for analysis of local orientation and for proofreading over aligned volumes. The pipeline is scalable, and combined with recent advances in experimental approaches, should enable new studies of mesoscale connectivity and function over the whole human brain.

Introduction

Our knowledge of connectivity in the human brain is limited by the lack of high-resolution tools to study individual white-matter axons over long distances. Even the statistics of axon trajectories has not been studied with methods that can resolve individual axons. Studies of human brain organization have focused on mapping whole brains at low resolution, e.g. with diffusion MRI (Glasser et al. 2016); but see (Walsh et al. 2021), or mapping small brain regions at extremely high resolution, e.g. with electron microscopy (Shapson-Coe et al. 2024), due to a lack of approaches that can both resolve individual axons and scale to the entire human brain. We have been developing an approach, axonal connectomics, that builds on high-resolution, high-speed acquisition of fluorescently labeled *ex vivo* tissue samples using a combination of light-sheet fluorescence and tissue expansion microscopy. At scale, axonal connectomics holds the promise of mapping both the local statistics and the long-distance targets of axon trajectories through white matter over entire human brains.

Despite significant advances in experimental methods, crucially, computational approaches to generating dense projection maps from the image data are needed. Major impediments to computing such maps include limitations of tissue processing and of the volumetric field-of-view of imaging systems, which preclude “single-shot” imaging of large brain volumes as physically intact samples. Analogous to serial section approaches in EM connectomics (Yin et al. 2020), the sample is first cut into sections in preparation for imaging, and subsequently, each section is imaged in a tiled acquisition from which the data must be montaged and reassembled into a volume *in silico* corresponding with the original sample. Furthermore, the problem of registering axons within a volume deformed by physical slicing, manipulation, and chemistry must be made solvable for datasets on the petavoxel scale.

We have developed a scalable computational pipeline for reconstructing and tracing axons for whole-brain axonal connectomics, building on progress in machine learning (ML)-based automated segmentation and tracing of axons (Gliko et al. 2024) and in petascale 3D registration and assembly of serially sectioned volumes (Mahalingam et al. 2022). In a departure from other approaches to volume assembly in both electron microscopy and light microscopy, we explored the use of early ML segmentation of individual tiles to generate skeletons of axons, thus reducing the image data and segmentation associated with axons to 1-d manifolds with a boundary, and enable computing with skeleton-based features. By providing skeletons as early inputs to volume assembly rather than a later downstream output, traces are available for feature-detection and volume registration, as well as for automated QC and targeted proofreading of the assembled volume. By computing with skeletons, the overall pipeline also benefits from fewer reading, processing, and rendering operations of high-dimensional image data. We demonstrate high-quality segmentation and skeletonization of dense axons, and demonstrate the use of this early skeletonization to volume assembly and scalable, automated tracing over serial sections.

Results

Description of axonal connectomics pipeline

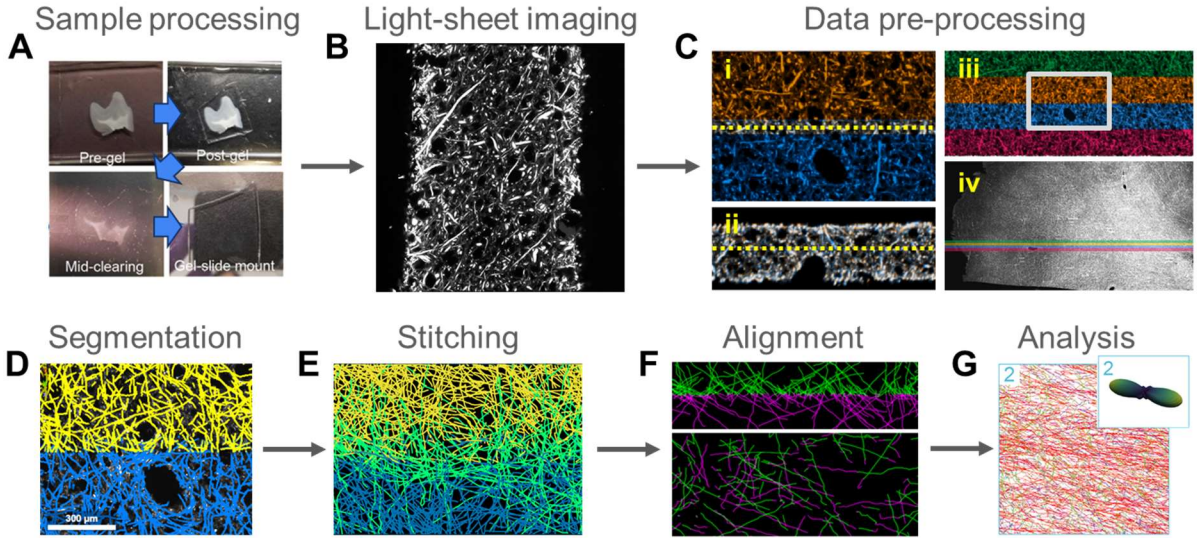

Figure 1: Pipeline for dense axon tracing over serially sectioned volumes
(**A**) Gelling, clearing, and expansion stages of tissue processing of immunostained sections. (**B**) Example fluorescence image from an expanded section acquired on an inverted light-sheet microscope. (**C**) Examples of adjacent, overlapping tiles (blue and yellow) after pre-processing image data into 3D volumes; (i): xy-plane sliced through dashed line in (ii); (ii): xz-plane sliced through dashed line in (i); (iii): set of 4 tiles with panel (i) shown in boxed region; (iv): zoomed out view of all section tiles with tiles in panel (iii) colored. (**D**) Example of axon traces segmented from blue and yellow tiles from (C). (**E**) Example of merged axons (green) stitched across blue and yellow tile boundaries. (**F**) Example of axon traces from two serial sections (green and magenta) aligned across their interface as viewed in the xz (top) and xy (bottom) planes. (**G**) Example of analysis of local axon orientation statistics.

Tissue enters the data acquisition pipeline as sections which have been chemically fixed and immunostained for neurofilament proteins which densely label axons. These sections are highly scattering initially, but through a combination of tissue clearing and expansion steps adapted from standard expansion microscopy (ExM) protocols (Tillberg et al. 2016; Ku et al. 2020), proteins of interest are anchored to a hydrogel matrix while the surrounding tissue is digested and homogenized, rendering the sections optically clear (Fig. 1A). The hydrogel expands isotropically to 4x in water, enabling fluorescence imaging of axons with effective resolution better than the optical diffraction limit. Expanded tissue is imaged on a custom inverted selective plane illumination microscope (iSPIM) (Wu et al. 2011) in which the light-sheet and image plane are tilted such that the images are oblique cross-sections of the sample (Fig. 1B). By scanning the sample through the light-sheet while simultaneously imaging, the microscope acquires a 3D volume analogous to a z-stack in standard fluorescence microscopy, albeit with a skewed geometry. After imaging, the image tiles, or “strips,” are deskewed into Cartesian 3D volumes with nearly isotropic voxels of dimension 0.8 μm x 0.8 μm x 0.7 μm which corresponds to an effective resolution of 0.2 μm x 0.2 μm x 0.175 μm in unexpanded tissue. The deskewed tiles are stored in a next-generation file format, OME-Zarr (Moore et al. 2023), as multi-resolution pyramids with metadata recording the stage position and acquisition parameters used to place each tile volume in the coordinate system of the full section (Fig. 1C). This preprocessed data volume serves as the input to the tracing and assembly pipeline.

The computational pipeline encompasses a set of tools for segmentation, stitching, registration, transformation, and visualization of large image data, integrated into a modular workflow. Strips are first individually segmented, and the segmentation is skeletonized to generate traces of axons (Fig. 1D). Axon traces from adjacent strips are stitched in overlapping regions between tiles and merged across tile boundaries to register skeletons in a montaged section volume (Fig. 1E). Sections are aligned by matching and computing transformations to connect axon endpoints at surface interfaces (Fig. 1F). The outputs of the pipeline are the transformations needed for the registration of skeletons from disparate image tiles and sections into an assembled 3D volume, along with the sets of correspondences generating the transformations. The registered traces thus become available for proofreading and analysis (Fig. 1G).

Automated segmentation and axon extraction

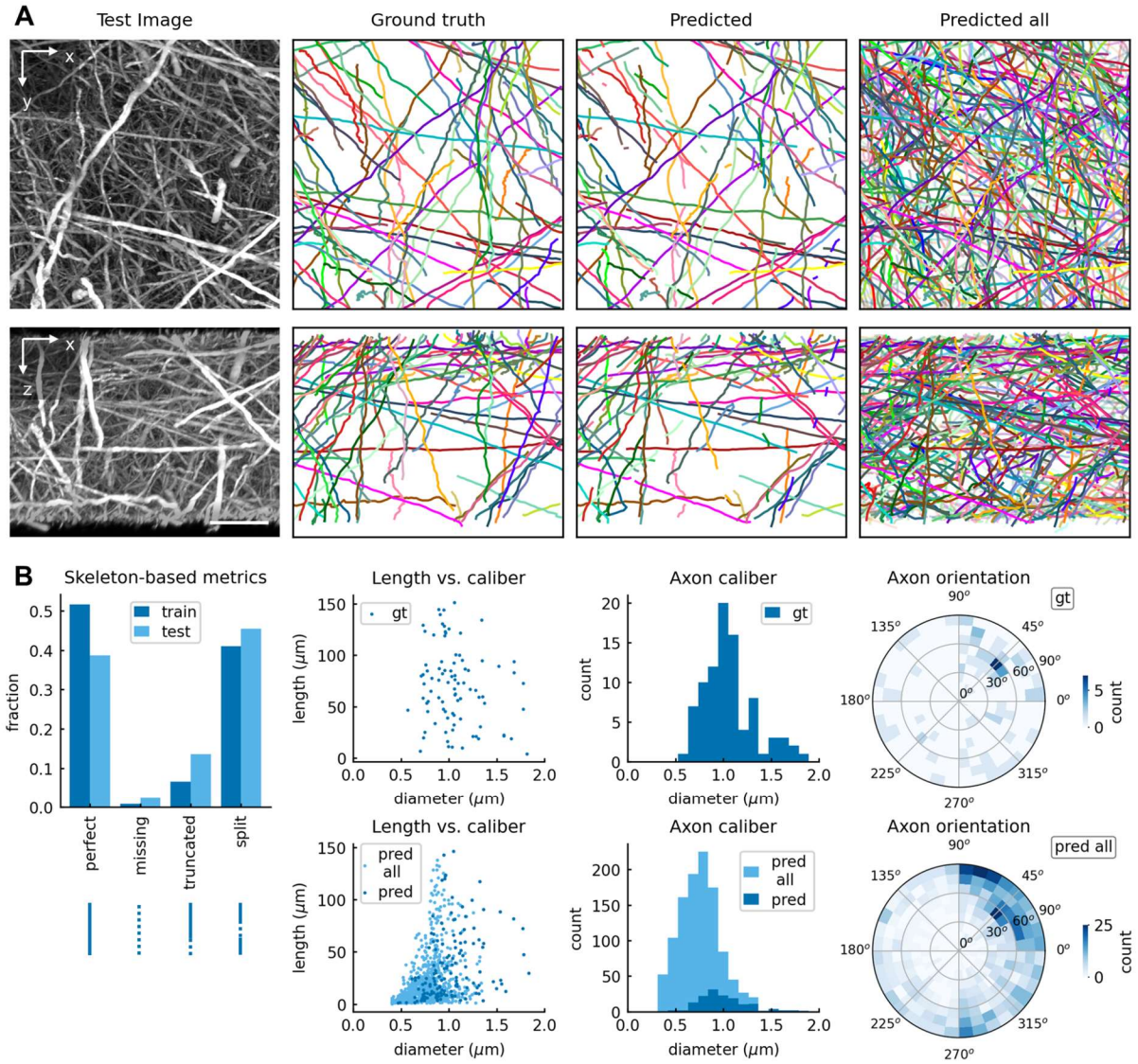

Figure 2: Automated axonal segmentation.
(**A**) Segmentation of testing dataset: xy- and xz- maximum intensity projections of image stack (left column), corresponding plots of ground truth (gt) axons (second column), predicted axons matching gt (third column), and all predicted axons (right column). Different colors indicate different connected components (same color for the segments of split predicted axons matching gt). Scale bar, 25 μm. (**B**) Comparison of predicted and gt axons: skeleton-based metrics for training and testing dataset (left column), axon length vs. caliber for gt (second column, top) and predicted axons (bottom), caliber of gt (third column, top) and predicted axons (bottom), orientation (polar vs. azimuth angle heatmap) of gt (right column, top) and predicted axons (bottom).

Our semi-automated (multi-step) approach for axonal reconstruction includes neural network-based segmentation followed by postprocessing and proofreading. The segmentation part of the computational pipeline uses OME-zarr image data of variable resolution as inputs and swc files as outputs, and allows generation of axon skeletons over entire sections. While proofreading is required for analysis of long-range axonal projections across the entire brain, it is not necessary for the section aligning process.

Axonal segmentation from 3-d image stacks requires generating a voxel-wise annotation, like the one used for EM segmentation (Lee et al. 2021). Since it is a very laborious task, we use a more time-efficient iterative approach by first segmenting dense axon image set using an existing model trained with sparse neuron image sets (Gliko et al. 2024). We then use a neuron tracing interface, CATMAID (Saalfeld et al. 2009), to proofread automated skeletons and generate an initial set of ground truth skeletons. We use a topology-preserving fast marching algorithm to generate volumetric labels from proofread skeletons and image data (Gliko et al. 2024). Using these label and image sets as training data and employing data augmentation including flips/rotations by 90° in the image (XY) plane, brightness and contrast variations, we train a convolutional neural network (U-Net) to produce a voxel-based axonal segmentation. We use an efficient Pytorch implementation that runs on graphical processing units (GPUs) and train the model on batches of 3-d patches (128 x 128 x128 px^3) with a GeForce GTX 1080 GPU using the Adam optimizer with a learning rate of 0.1. With this approach we are able to further refine the segmentation model with larger and more diverse datasets.

We algorithmically post-process the initial voxel-based segmentation by thresholding the background, followed by connected component analysis to remove short segments, skeletonization with Kimimaro (Silversmith et al. 2021), conversion to digital reconstruction in swc format, and assigning a radius to every node. These initial small segments accurately capture axonal trajectories as assessed by human inspection, but contain topological errors such as false merges. The skeletons are therefore split at branch points, resulting in short linear segments, similar to the initial oversegmentation of EM data (Lee et al., 2021). We use the ground truth skeletons to train a classifier that learns a merging score, based on computed features for all pairs of nearby axonal segments. Segments are then iteratively merged, starting with the pairs with the highest score, reaching a conservative threshold chosen to minimize errors while increasing the mean length. This automated approach dramatically decreases the number of topological errors while reducing the proofreading time (Fig. 2A). We evaluate the quality of automated axonal reconstructions by comparing them to ground truth axons. Since only a limited part of axons was proofread, we select predicted axons with nodes that have corresponding nodes in ground truth within a distance of 2 voxels. We quantify the reconstruction accuracy using skeleton-based metrics as a fraction of ground truth axons being perfect, missing, truncated or split. We report these metrics for training and testing datasets (Fig. 2B). The number of splits per axon is in the 1-4 (1-8) range for testing (training) sets. We report an axonal segment as truncated if its length is below 90% of the length of ground truth axon and as split if it is both split and truncated. We do not report false merges due to incomplete ground truth, though we did not find any false merges by manual inspection of the test dataset. In addition, we found good correspondence between axon length, caliber and orientation for predicted and ground truth axons. Subsequent proofreading is performed to correct split errors and extend axon fragments into longer segments. Our proofreading on millimeter-scale regions of sections showed that >90% of axons can be traced to the edges of the volume, including the top and bottom surfaces of the section. This includes axons <1 μm in diameter, while a larger majority of the >1 μm axons are unbroken. This preliminary run-length analysis will form the backbone of our quality control metrics.

Stitching tiles into sections

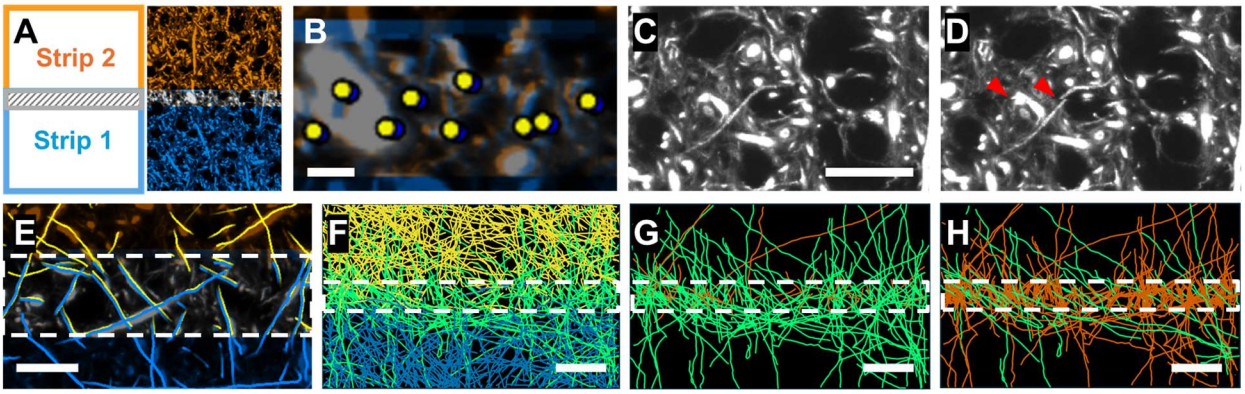

Figure 3: Automated stitching of axons within sections.
(**A**) Schematic and example of overlapping strip acquisitions. (**B**) Stitching point correspondences generated in the overlap region. Scale bar, 20 µm. (**C**) Fully stitched image data at the boundary between tiles. Scale bar, 50 µm. (**D**) Comparison of same boundary in C without stitching (stage position metadata only) showing visibility of seams (arrows). (**E**) Stitched image data and skeletons in the overlap region between tiles (dashed lines). Scale bar, 50 µm. (**F**) Stitched skeletons merged across tile boundary (green) with skeletons from adjacent yellow and blue strips. (**G**) Merged skeletons (green) compared with unmerged skeletons present in the overlap region (red) from panel F. (**H**) Merged (green) and unmerged (red) skeletons in the overlap region from panel F without stitching. Scale bars, 100 µm.

Imaging of a large section is performed in tiles which must be co-registered to form a montage of the section in its entirety. For our image acquisition, a single section is tiled as a series of "strips," each of which is generated by a unidirectional scan line along the x-axis of the stage and spaced across the y-axis such that ~10% of the field-of-view overlaps between tiles for stitching (Fig. 3A). Due to inaccuracies of stage motion and other sources of uncertainty such as sample drift, the position of one tile in the imaging volume relative to another may deviate from the intended sample positioning. The stitching module generates and stores the output of stitching as metadata encompassing correspondences between spatial points in one tile with those of an adjacent neighbor and the set of transforms which register these point correspondences (Fig. 3B). These correspondences can be produced through a variety of standard image analysis techniques including correlation and template matching, as well as feature detection-based methods, but more generally, could be generated from more complicated representations, such as from neural networks and machine learning. Here, we use a multi-resolution combination of SIFT features (Lowe 1999) and cross-correlation for generation of stitching correspondences, and use colocalization of the ML-generated skeletons for parameter optimization and QC. The quality of stitching is commonly assessed from visualization and analysis of continuity of the transformed and rendered image data, and from identification of stitching-related artifacts, such as seams (Fig. 3C-D). The use of the skeletons for stitching validation enables automated QC and directly reports projection mapping errors. Although minor misalignments may be visually subtle, they may still impact skeleton merging across tiles, which assumes near-complete overlap of the image data. Indeed, after transformation with the stitching translations determined from the image-derived correspondences, skeletons in the overlap region are expected to colocalize identically with the

image data (Fig. 3E). Close alignment allows merging of the subset of skeletons that cross the tile boundaries by cutting skeletons at intersection points and joining the cut ends (Fig. 3F). Due to variability in the segmentation output between strips, as well as potential residual misalignment, a typically small fraction of skeletons present in the overlap region remain unmerged (Fig. 3G). Errors and failures of stitching are identifiable as a significant increase in the fraction of unmerged boundary skeletons (Fig. 3H), providing an intrinsic control on the quality of stitching.

Assembling sections into volumes

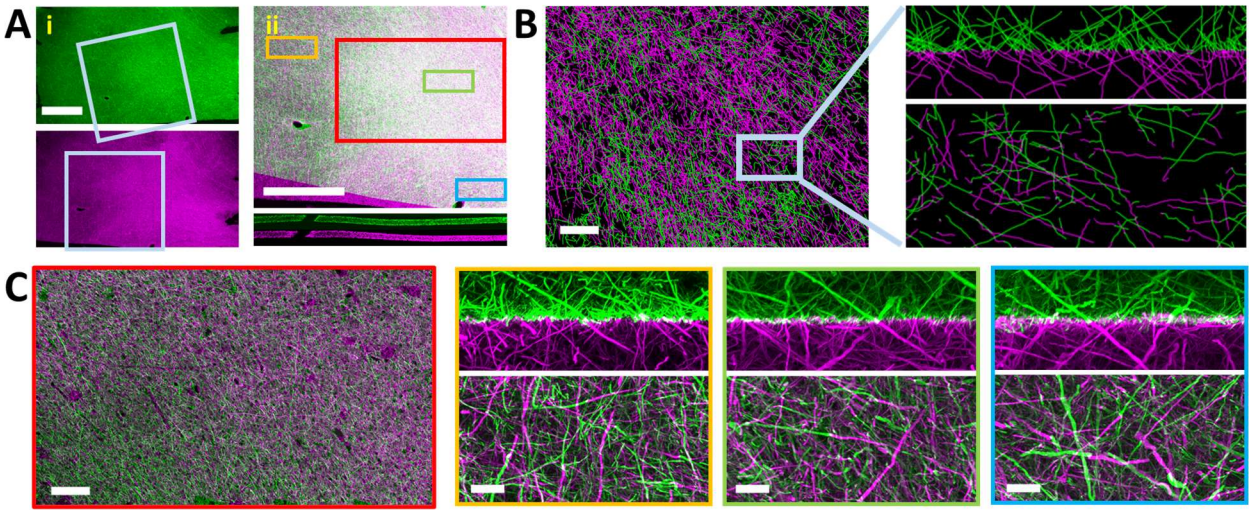

Figure 4: Automated registration and tracing of axons between serial sections
(**A**) Coarse registration of serial sections determined by matching large features (blood vessels); i: zoomed-out views of serial sections of human cortex (green, top, and magenta, bottom) with boxed field-of-view showing relative rotation; ii: zoom-in of coarse registration of boxed regions in panel (i) as viewed from the top (xy-slice, top) and from the side (xz-slice, bottom). Scale bar, 5 mm. (**B**) Skeletons from serial sections in A matched, transformed, and aligned at the flattened section interface. Zoom-ins of aligned skeletons in the boxed region are shown on the right as viewed in the xz (top) and xy (bottom) planes. Scale bar, 1 mm. (**C**) Left: volume renderings of the transformed image data showing alignment of axons across the slice interface from the large boxed, white-matter area (red) in A, scale bar: 1 mm. Right: small boxed regions outlined in yellow, green, and blue in A, scale bars: 100 µm.

The most challenging step in volume assembly is the unification of serial sections by tracing axons between slices. Our approach to inter-section alignment uses the endpoints of axon skeletons at the surfaces of adjacent sections for pairing skeletons split across the interface. Endpoint correspondences are generated using an iterative registration process between sub-regions of the dataset, flattened using a surface estimation, then jointly registered (Saalfeld et al. 2010; Khairy, Denisov, and Saalfeld 2018) using a progressively regularized set of 2D transformations as described in the ASAP volume assembly pipeline (Mahalingam et al. 2022). First, highly downsampled image data (20 µm voxels) are used for the initial determination of a global rigid (rotation + translation) transform based on coarse registration of large anatomical landmarks such as major blood vessels and for automated detection of the tissue surfaces (Fig. 4A). This registration and surface mapping step allows filtering of skeletons with endpoints near to the surface and projection of their endpoint coordinates into globally registered 2D planes.

Endpoints within each subregion of the coarsely registered section interface are iteratively matched by running corresponding nearest neighbor and angle of impact metrics through random sample consensus (RANSAC) regression targeting a similarity to produce a stable set of inliers. For larger or more deformed subregions, as well as a way to enforce consistency between subregions, an iterative approach to robust RANSAC allows greater coverage of correspondences while encompassing more local transformations (Saalfeld et al. 2012). The stable set of correspondence inliers across the section interface serves as input to a global alignment process solving across all section interfaces for increasingly regularized global rotational, affine, and grid-deformed thin-plate spline transformations. This composite nonlinear transformation connects the endpoints of correspondences set and can be applied to all endpoints at the section interface (Fig. 4B). If the section volume is sufficiently flat or is computationally flattened, the transformation can further be applied to the image data slice-by-slice for a volumetric alignment. Transformation of the entire image data volume is not strictly necessary for the output of the pipeline given the connected traces are the primary output of section alignment, and nonlinear warping and rendering of the high-resolution data adds considerable computational and infrastructural cost if performed generally. Nevertheless, transformations for very large regions can be generated by combining endpoint correspondences over sub-regions of interest, and more practically, transformations can be applied locally to small volumes for targeted rendering, validation, and proofreading (Fig. 4C and Supplementary Movies 1-2).

Exploratory analysis of local statistics of axon orientation (and proofreading of output)

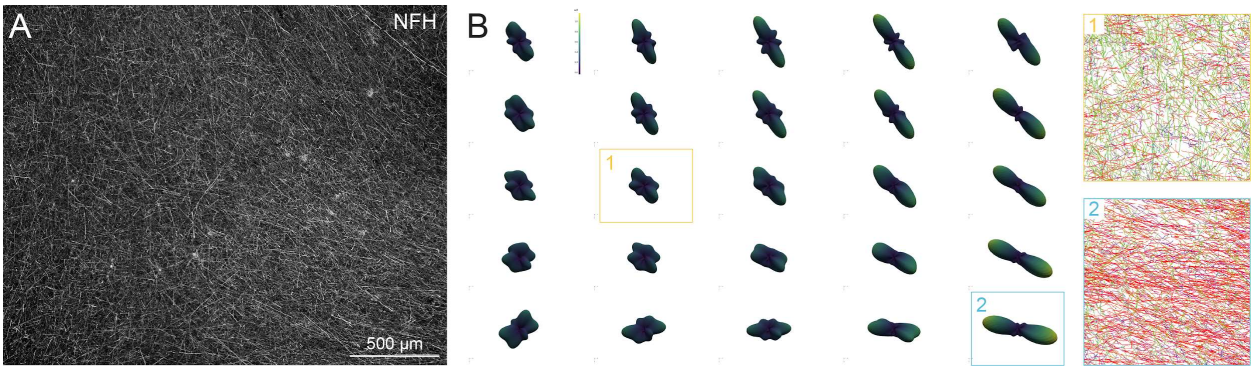

Figure 5: Analysis of local orientation of individual axons
(**A**) Max-z projection view of image stacks from the visual cortex of human tissue covering about 2.5 x 2.5 x 0.12 mm pre-expansion, immunostained with neurofilament heavy-chain. Scale bar, 500 µm. (**B**) Left column: Orientation density function of segmented skeletons in each of 500 x 500 x 0.12 mm subregions. Zoomed-in views of skeletons in two selected regions are shown in the right column. Skeletons are colored by their orientation (orientation vector mapped to RGB space).

Following the complete computational pipeline for segmentation of densely labeled axons and image volume assembly, significant efforts in proofreading are required to trace individual axons by connecting pieces of split skeletons. Here, we present an exploratory analysis of local

statistics of axon trajectory orientations using segmented skeleton data in the visual cortex of the human brain.

The max-z projection image of neurofilament immunostaining demonstrates densely labeled axon fibers interposed with each other (Fig. 5A). This region of interest was divided into 5x5 subregions, each covering approximately 500 x 500 micrometers in the xy plane. For each subregion, the orientation distribution function was estimated (Fig. 5B, left) based on the tangent vectors of skeleton segments within that region (Trinkle et al. 2021).

The analysis reveals a general global axonal trajectory from the lower right to the upper top. However, not all subregions exhibit a dominant axonal fiber orientation. In regions without a dominant fiber orientation (Fig. 5B, orange box), the orientation distribution is more uniform, indicating a more random arrangement of axonal trajectories. Even in regions with a dominant fiber orientation (Fig. 5B, blue box), there is still a significant number of axons that do not conform to the primary direction, highlighting the complexity and variability in axonal organization.

Discussion

Comparisons with other approaches

The axonal connectomics tracing and assembly pipeline was designed to be a scalable and modular approach to generating dense projection maps from large, serially sectioned samples. The most similar alternatives to our knowledge are the serial sectioning and clearing, three-dimensional microscopy with semi-automated reconstruction and tracing (SMART) pipeline developed by the Bi group (Xu et al. 2021) and the Unification of Neighboring Sliced-tissues via Linkage of Interconnected Cut fiber Endpoints (UNSLICE) method developed by the Chung group (Park et al. 2023). The SMART approach in particular has demonstrated scalability to processing of entire primate brains; however, the pipeline was developed for comparatively sparse labeling of projections by viral injection and leverages sparsity in its alignment processing. The UNSLICE approach in contrast is able to align dense projections across serial sections but also requires co-staining of multiple molecular species and vasculature to perform step-wise registration in successive rounds of increasing accuracy with different imagery. An important distinction between these alternatives and the approach described here is the dense segmentation of axons providing high-quality traces for skeleton-based processing early in the pipeline and consequently, the primary role the segmentation plays in volume assembly. With the goal of projection mapping over large brains, we aimed to automate processing and validation with the traces as much as possible, and similarly minimize requirements for excess data acquisition and storage, as well as for processing of the raw image data. Given the difficulty and expense of acquiring, storing, managing, and processing extremely large data volumes, the scalability of our pipeline benefits from the economy of relying mainly on the processing of low-dimensional skeletons from only a single channel of data. Additional channels may still be acquired for non-alignment purposes, but each additional dataset comes at

significant cost of increases in sample acquisition time and/or complexity, and computational and infrastructural burden.

Several published stitching software packages for large datasets are openly available (Hörl et al. 2019; Bria and Iannello 2012; Ruan et al. 2024). Existing stitching packages provide an integrated solution for both generating transformations and transforming the image data to render a “stitched” dataset. In our pipeline, the latter rendering step is a distinct process which we chose to avoid in many cases. Rendering stitched intermediates for processing was expensive and generally unnecessary given the existing segmentation and traces which we also aimed to leverage in the computation and validation of the stitching output. Thus, we implemented the lightweight stitching module described above with additional features for skeleton-based processing and QC. However, a key benefit of the modular design is that it is straightforward to substitute in the correspondences and transformations generated by another stitching package, which provides the opportunity for alternative implementations and further optimization in future development.

Future directions

While our current segmentation captures the majority of axons and postprocessing allows us to correct a significant amount of false split/merge mistakes, much further improvement is needed to achieve more accurate tracing of axons. We expect to achieve significant improvement of segmentation accuracy by using larger and more diverse training data and employing affinity-based models with connectivity-preserving objective functions. In addition, our current approach for linking axonal segments obtained by splitting the branching nodes can be improved by training a graph neural network, where the nodes represent axonal segments and edge attributes capture relative position information, such as orientation and distance between a pair of segments.

The pipeline was built upon computational tools from the ASAP package developed for petascale volume assembly out of 2D image tiles from EM. In contrast, the image tiles acquired by the light-sheet microscope represent 3D volumes in themselves, and generally exhibited 3D deformations out of the plane which required supplementing the EM methods with modules for surface detection and flattening. Adaptations of EM tools were suitable for the projection mapping approach described here, namely the detection and registration of correspondences between axon traces across image tiles and section interfaces. However, the present pipeline does not support generalized volumetric transformations which becomes a limitation when aligning sections with severe surface curvature. We are currently investigating scalably extending our transformation models to handle 3D deformations.

We validated the proof-of-principle of segmentation-driven alignment by constructing the pipeline described above and applying it to axon tracing across a preliminary dataset of two serial sections. In a much larger effort combining multiple technical advances in sample preparation and imaging methods with the computational pipeline developed here, we are performing projection mapping over a volume at scale. As noted in the introduction, the problems of scaling include lifting constraints of sample preparation and of the field-of-view of

imaging, which have been addressed by improvements in staining, clearing, and expanding thick sections and by recent innovation in light-sheet imaging technology (Glaser et al. 2023), respectively. The successful integration and demonstration of a fully scaled axonal connectomics pipeline promises to break new ground in our understanding of the connectivity of large mammalian brains, particularly through the white matter, and will advance our understanding of human brain anatomy and cognition.

References and Acknowledgements

Bria, Alessandro, and Giulio Iannello. 2012. "TeraStitcher - a Tool for Fast Automatic 3D-Stitching of Teravoxel-Sized Microscopy Images." *BMC Bioinformatics* 13 (November): 316.

Glaser, Adam, Jayaram Chandrashekar, Joshua Vasquez, Cameron Arshadi, Naveen Ouellette, Xiaoyun Jiang, Judith Baka, et al. 2023. "Expansion-Assisted Selective Plane Illumination Microscopy for Nanoscale Imaging of Centimeter-Scale Tissues." *ELife*. https://doi.org/10.7554/elife.91979.1.

Glasser, Matthew F., Timothy S. Coalson, Emma C. Robinson, Carl D. Hacker, John Harwell, Essa Yacoub, Kamil Ugurbil, et al. 2016. "A Multi-Modal Parcellation of Human Cerebral Cortex." *Nature* 536 (7615): 171–78.

Gliko, Olga, Matt Mallory, Rachel Dalley, Rohan Gala, James Gornet, Hongkui Zeng, Staci Sorensen, and Uygar Sümbül. 2024. "High-Throughput Analysis of Dendritic and Axonal Arbors Reveals Transcriptomic Correlates of Neuroanatomy." *BioRxiv*. https://doi.org/10.1101/2022.03.07.482900.

Hörl, David, Fabio Rojas Rusak, Friedrich Preusser, Paul Tillberg, Nadine Randel, Raghav K. Chhetri, Albert Cardona, et al. 2019. "BigStitcher: Reconstructing High-Resolution Image Datasets of Cleared and Expanded Samples." *Nature Methods* 16 (9): 870–74.

Khairy, Khaled, Gennady Denisov, and Stephan Saalfeld. 2018. "Joint Deformable Registration of Large EM Image Volumes: A Matrix Solver Approach." *ArXiv [Cs.CV]*. arXiv. http://arxiv.org/abs/1804.10019.

Ku, Taeyun, Webster Guan, Nicholas B. Evans, Chang Ho Sohn, Alexandre Albanese, Joon-Goon Kim, Matthew P. Frosch, and Kwanghun Chung. 2020. "Elasticizing Tissues for Reversible Shape Transformation and Accelerated Molecular Labeling." *Nature Methods* 17 (6): 609–13.

Lee, Kisuk, Ran Lu, Kyle Luther, and H. Sebastian Seung. 2021. "Learning and Segmenting Dense Voxel Embeddings for 3D Neuron Reconstruction." *IEEE Transactions on Medical Imaging* 40 (12): 3801–11.

Lowe, D. G. 1999. "Object Recognition from Local Scale-Invariant Features." In *Proceedings of the Seventh IEEE International Conference on Computer Vision*, 2:1150–57 vol.2. IEEE.

Mahalingam, Gayathri, Russel Torres, Daniel Kapner, Eric T. Trautman, Tim Fliss, Shamishtaa Seshamani, Eric Perlman, et al. 2022. "A Scalable and Modular Automated Pipeline for Stitching of Large Electron Microscopy Datasets." *ELife* 11 (July). https://doi.org/10.7554/eLife.76534.

Moore, Josh, Daniela Basurto-Lozada, Sébastien Besson, John Bogovic, Jordão Bragantini, Eva M. Brown, Jean-Marie Burel, et al. 2023. "OME-Zarr: A Cloud-Optimized Bioimaging File Format with International Community Support." *BioRxiv : The Preprint Server for Biology*, May. https://doi.org/10.1101/2023.02.17.528834.

Park, Juhyuk, Ji Wang, Webster Guan, Lars A. Gjesteby, Dylan Pollack, Lee Kamentsky, Nicholas B. Evans, et al. 2023. "Integrated Platform for Multi-Scale Molecular Imaging

and Phenotyping of the Human Brain." *BioRxiv*. https://doi.org/10.1101/2022.03.13.484171.
Ruan, Xiongtao, Matthew Mueller, Gaoxiang Liu, Frederik Görlitz, Tian-Ming Fu, Daniel E. Milkie, Joshua L. Lillvis, et al. 2024. "Image Processing Tools for Petabyte-Scale Light Sheet Microscopy Data." *BioRxiv*. https://doi.org/10.1101/2023.12.31.573734.
Saalfeld, Stephan, Albert Cardona, Volker Hartenstein, and Pavel Tomancak. 2009. "CATMAID: Collaborative Annotation Toolkit for Massive Amounts of Image Data." *Bioinformatics* 25 (15): 1984–86.
Saalfeld, Stephan, Albert Cardona, Volker Hartenstein, and Pavel Tomančák. 2010. "As-Rigid-as-Possible Mosaicking and Serial Section Registration of Large SsTEM Datasets." *Bioinformatics* 26 (12): i57-63.
Saalfeld, Stephan, Richard Fetter, Albert Cardona, and Pavel Tomancak. 2012. "Elastic Volume Reconstruction from Series of Ultra-Thin Microscopy Sections." *Nature Methods* 9 (7): 717–20.
Shapson-Coe, Alexander, Michał Januszewski, Daniel R. Berger, Art Pope, Yuelong Wu, Tim Blakely, Richard L. Schalek, et al. 2024. "A Petavoxel Fragment of Human Cerebral Cortex Reconstructed at Nanoscale Resolution." *Science* 384 (6696): eadk4858.
Silversmith, William, J. Alexander Bae, Peter H. Li, A. M. Wilson. 2021. *Seung-Lab/Kimimaro: Zenodo Release V1*. https://doi.org/10.5281/zenodo.5539913.
Tillberg, Paul W., Fei Chen, Kiryl D. Piatkevich, Yongxin Zhao, Chih-Chieh Jay Yu, Brian P. English, Linyi Gao, et al. 2016. "Protein-Retention Expansion Microscopy of Cells and Tissues Labeled Using Standard Fluorescent Proteins and Antibodies." *Nature Biotechnology* 34 (9): 987–92.
Trinkle, Scott, Sean Foxley, Narayanan Kasthuri, and Patrick La Rivière. 2021. "Synchrotron X-Ray Micro-CT as a Validation Dataset for Diffusion MRI in Whole Mouse Brain." *Magnetic Resonance in Medicine: Official Journal of the Society of Magnetic Resonance in Medicine / Society of Magnetic Resonance in Medicine* 86 (2): 1067–76.
Walsh, C. L., P. Tafforeau, W. L. Wagner, D. J. Jafree, A. Bellier, C. Werlein, M. P. Kühnel, et al. 2021. "Imaging Intact Human Organs with Local Resolution of Cellular Structures Using Hierarchical Phase-Contrast Tomography." *Nature Methods* 18 (12): 1532–41.
Wu, Yicong, Alireza Ghitani, Ryan Christensen, Anthony Santella, Zhuo Du, Gary Rondeau, Zhirong Bao, Daniel Colón-Ramos, and Hari Shroff. 2011. "Inverted Selective Plane Illumination Microscopy (*i*SPIM) Enables Coupled Cell Identity Lineaging and Neurodevelopmental Imaging in *Caenorhabditis Elegans*." *Proceedings of the National Academy of Sciences of the United States of America* 108 (43): 17708–13.
Xu, Fang, Yan Shen, Lufeng Ding, Chao-Yu Yang, Heng Tan, Hao Wang, Qingyuan Zhu, et al. 2021. "High-Throughput Mapping of a Whole Rhesus Monkey Brain at Micrometer Resolution." *Nature Biotechnology* 39 (12): 1521–28.
Yin, Wenjing, Derrick Brittain, Jay Borseth, Marie E. Scott, Derric Williams, Jedediah Perkins, Christopher S. Own, et al. 2020. "A Petascale Automated Imaging Pipeline for Mapping Neuronal Circuits with High-Throughput Transmission Electron Microscopy." *Nature Communications* 11 (1): 4949.

Acknowledgements

We wish to thank the Allen Institute for Brain Science founder, Paul G Allen, for his vision, encouragement, and support. This work was supported by the National Institutes of Health through award numbers R01MH117820 and UG3MH126864 (PI: Reid).

Author contributions

R.T., K.T., O.G., and C.R. conceived the pipeline. R.T., K.T., O.G., C.L., and W.Q.Y. contributed pipeline code, results, and analysis. E.T. prepared human histological sections. A.H. provided ground truth and proofreading. P.B., E.P., and U.S. provided methodology. All authors contributed to the manuscript.